High-pressure sliding using rod samples for grain refinement and superplasticity in Al and Mg alloys

T. Masuda[1], K. Fujimitsu[1], Y. Takizawa[1,2], Z. Horita[1,2†]

†horita@zaiko.kyushu-u.as.jp

[1]Department of Materials Science and Engineering, Faculty of Engineering, Kyushu University, Fukuoka 819-0395, Japan
[2] WPI, International Institute for Carbon-Neutral Energy Research, Kyushu University, Fukuoka 819-0395, Japan

High-pressure sliding (HPS) is a process of severe plastic deformation (SPD) for significant grain refinement and it is similar to high-pressure torsion (HPT) as both processes are operated under high pressure. Whereas the HPT process uses disk or ring samples, the HPS process is applicable to rectangular sheet samples. In this study, it is demonstrated that the HPS process is also applicable to rod samples. To achieve a homogeneous microstructure throughout the cross section of the rod, the sample is rotated along the longitudinal axis after each processing. The HPS process is carried out on pure Al, Al alloys (Al-3%Mg-0.2%Sc, A2024 and A7075) and a Mg alloy (AZ61) under a pressure in the range of 1-2 GPa. It is shown that a homogeneous microstructure is developed in all samples through rotation along the longitudinal axis by 60 degrees after each processing. The Al alloys and the Mg alloy exhibit grain sizes well less than 500 nm and superplastic elongation well more than 400% for the A2024 and A7075 alloys and well more than 1000% for the Al-3%Mg-0.2%Sc alloy and the AZ61 alloy. It is thus antgicipated that the HPS process provides good potential for scaling-up the sample size through not only sheets but also rods.

Keywords: severe plastic deformation (SPD), ultrafine grains (UFG), superplasticity, Vickers hardness, tensile test

Скольжение под высоким давлением прутковых образцов для измельчения зерен и сверхпластичности сплавов Al и Mg

Скольжение под высоким давлением (СВД) представляет собой процесс интенсивной пластической деформации (ИПД) для значительного измельчения зерен и аналогичен кручению под высоким давлением (КГД), поскольку оба процесса осуществляются под высоким давлением. Тогда как процесс КВД использует образцы в виде диска или кольца, СВД применяется к образцам в форме прямоугольных листов. В настоящей работе показано, что процесс СВД может быть применен также к прутковым образцам. Чтобы достичь однородной микроструктуры по всему поперечному сечению прутка, последний поворачивается вокруг своей продольной оси после каждой обработки. Процесс СВД проведен на чистом Al, алюминиевых сплавах Al-3%Mg-0.2%Sc, А2024 и А7075, а также на магниевом сплаве AZ61 под давлением в интервале 1-2 ГПа. Показано, что во всех образцах формируется однородная микроструктура путем поворота вокруг продольной оси на 60° после каждой обработки. Алюминиевые сплавы и сплав магния демонстрируют измельчение зерен до размеров менее 500 нм и сверхпластические удлинения значительно выше 400% для сплавов А2024 и А7075 и более 1000% для сплавов Al-3%Mg-0.2%Sc и AZ61. Таким образом, можно ожидать, что процесс СВД имеет потенциал масштабирования размеров образцов не только на листовые, но и на прутковые образцы.

Ключевые слова: интенсивная пластическая деформация (ИПД), ультрамелкие зерна (УМЗ); сверхпластичность; твердость по Виккерсу; испытание растяжением

1. Introduction

Grain refinement is an important requirement for achieving superplasticity [1]. This requirement is well fulfilled by application of severe plastic deformation (SPD) as the grain size is generally reduced to the submicrometer or nanometer range in metalic materials [2,3]. Several processes are available for the SPD process [3] and, among them are equal-channel angular pressing (ECAP) [4], accumaltive roll bonding (ARB) [5] and high-pressure torsion (HPT) [6]. The ECAP process is good for rods, the ARB for sheets and the HPT for disks and rings. The HPT process has an advantage over the others as it is applicable for hard and less ductile materials [7—9]. However, the samples size is limited in comarison with those for the ECAP and ARB processes, although there are attempts to modify the HPT
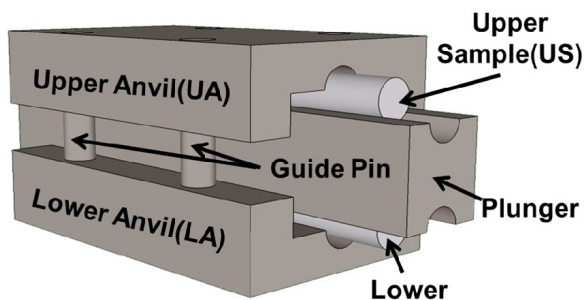
process so that it may may be continuous for wires and ribbons [10,11] or applicable to rods and tubes [12—15]. Recently, the method designated as high-pressure sliding (HPS) was introduced, which is applicable to rectangular sheets under high pressure [16]. Grain refinement to the submicrometer sizes was well achieved with the HPS process [17,18] and the superplasticity was sucessfully attained on Al and Mg alloys [17]. In this study, we show that the HPS process is applicable to rod samples to refine the grain size in the submicrometer range. This application includes not only pure Al and a superplastic Al-3%Mg-0.2%Sc alloy but also age-hardenable high-strength Al alloys such as A2024 and A7075 and a less ductlie Mg alloy such as AZ61. It is demonstrated that the grain size is significantly reduced and thus superplasticity is well attained in such alloys.

2. Experimental procedures

Rods with dimensions of 3mm diameter were prepared from ingots of pure Al (99.99%), an Al-3%Mg-0.2%Sc alloy, commercially extruded rods of aluminum A2024 and A7075 alloys, and a magnesium AZ61 alloy. The rods were cut to the lengths of 100 mm for the pure Al, Al-3%Mg-0.2%Sc alloy and AZ61 alloy and to the lengths of 50 mm for the A7075 alloy and of 60 mm for the 2024 alloy. Each sample was annealed (solution treated) at 773 K, 873 K, 793 K, 763 K and 773 K for pure Al, Al-3%Mg-0.2%Sc, A2024, A7075 and AZ61 alloys, respectively, for 1 hour except for the 7075 alloy which is for 5 hours. The grain sizes measured after the annealing (or solution treatment) are 290, 30, 60, 20, 30 μm, respectively, where the grain size of the 7075 alloy is for the short axis of elongated grains.

The rod samples were processed by an HPS facility as illustrated in Fig. 1. Two samples were placed between the anvils and plunger and, while applying loads between the upper and lower anvils, the plunger was pushed for a sliding distance of 10 mm for all samples (additionally 5 and 15 mm for pure Al) to introduce shear strain in the rods. The applied pressure was 1 GPa for pure Al and the Al-3%Mg-0.2%Sc alloy, 1.4 GPa for AZ61 and 2 GPa for A2024 and A7075. The HPS-processing temperature is at room temperature for all materials except for AZ61 which is 473 K. The processing speed is 3 mm/s for pure Al, 1.5 mm/s for the Al-3%Mg-0.2%Sc alloy, 2.5 mm/s for the A2024 and A7075 alloys and 0.2 mm/s for the AZ61 alloy.

Microstructures of the HPS-processed rods were observed by optical microscopy (OM) and transmission electron

microscopy (TEM) on the cross section perpendicular to the longitudinal axis at the mid length of the rod as illustrated in Fig. 2a. Vickers microhardness was also measured on the cross section covering the entire area with 0.25 mm apart each other as shown by dots in Fig. 2b. The measurement was made with applied loads of 50 g for 15 seconds for pure Al, Al-3%Mg-0.2%Sc and AZ 61, and of 200 g for 15 seconds for A2024 and A7075. The tensile specimen with dimensions as given in Fig. 2c was extracted at the mid length of the HPS-processed rods as also illustrated in Fig. 2a with the gauge part at the center of the cross section using an electrical discharge machine.

Tensile tests were conducted with an initial strain rate of 1×10^{-3} s^{-1}, 2×10^{-3} s^{-1} and 3×10^{-3} s^{-1} at a temperature in the range of 473—673 K.

In order to achieve a homogeneous development of microstructure, the rods were rotated around the longitudinal axis as illustrated in Fig. 3, where Fig. 3a is for 2 passes with 90° rotation after the first pass and Fig. 3b is for 3 passes with 60° rotation after each pass.
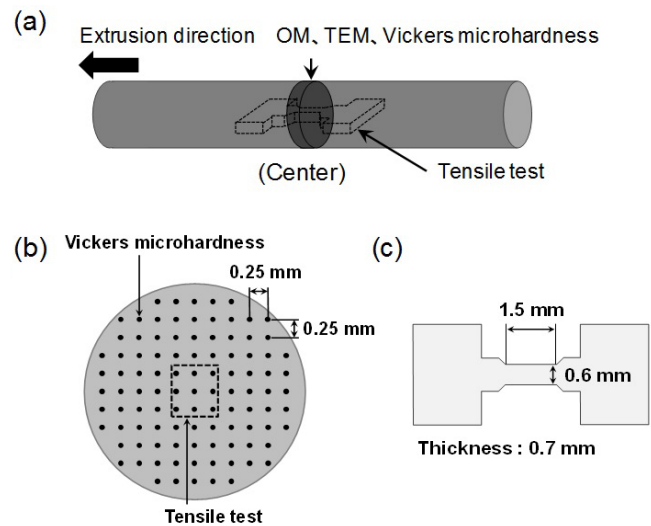

Fig. 2. Schematic illustrations of (a) sampling location for optical microscopy (OM), transmission electron microscopy (TEM), Vickers microhardness measurement and tensile testing, (b) positions for Vickers microhardness and cross sectional region at gauge part of tensile specimen, and (c) dimensions of tensile specimen.
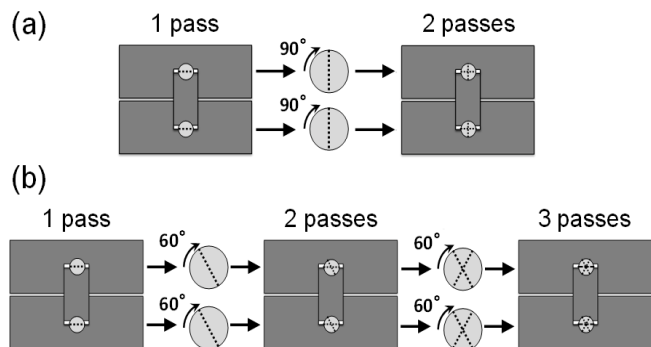
Fig. 3. Processing approaches for (a) 2 passes with 90o rotation around longitudinal axis and (b) 3 passes with 60o rotation around longitudinal axis.

Fig. 1. Schematic illustration of high-pressure sliding (HPS) for rod samples.

3. Results and discussion

Figure 4 shows OM micrographs and hardness variations (maps) of pure Al throughout the cross sections, where Fig. 4a is for 90° rotation after sliding for 5, 10 and 15 mm and Fig. 4b for 60° rotation after sliding for 5 and 10 mm. In Fig. 4a, regions with intense strain introduced across the diameter are visible with dark contrasts exhibiting «plus» marks on the cross sections and such plus contrasts become more prominent as the sliding distance increases. This trend
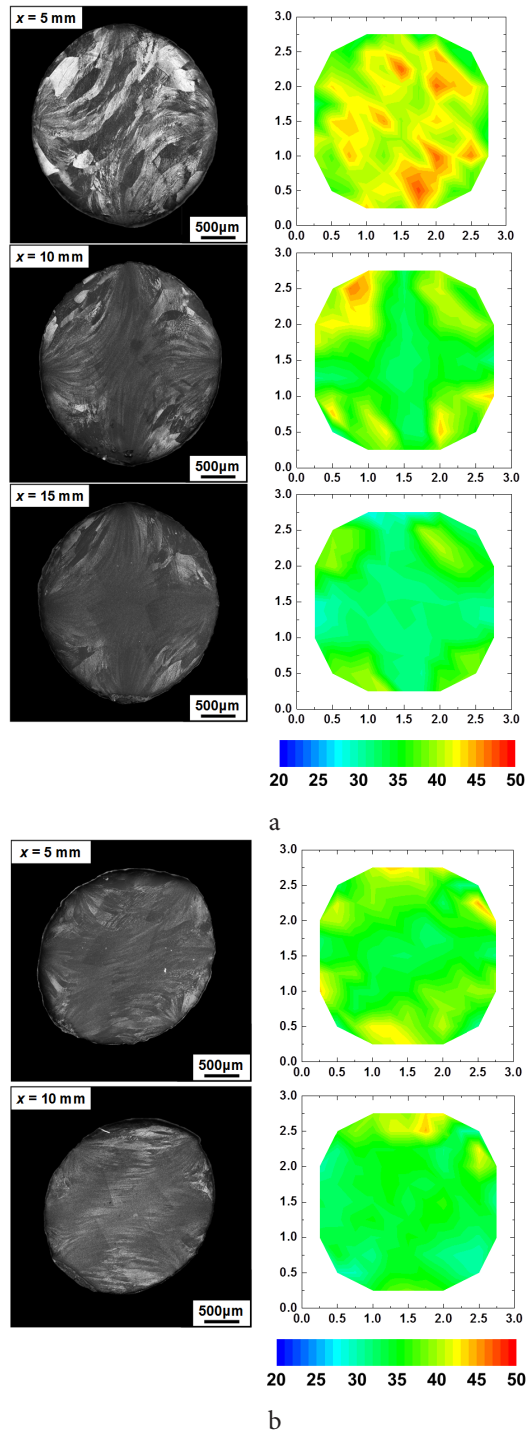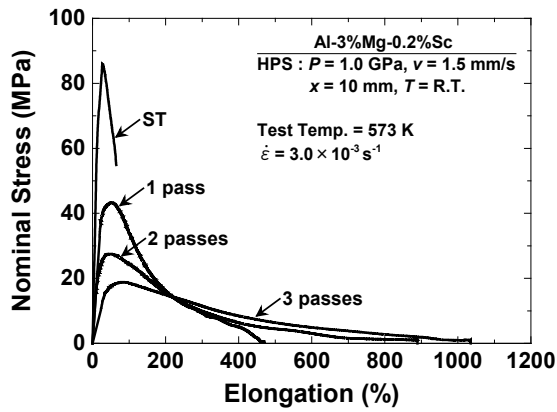
also appears in the hardness maps. It should be noted that in high purity Al in 99.99% as present, the hardness variation with respect to strain is peculiar such that the hardness increases to a maximum with straining but rather decreases with further straining as reported earlier [19—21]. Due to this peculiarity, the plus mark regions in the hardness maps become softer as the sliding distance increases. In Fig.4b, the dark contrast regions appear throughout the cross sections and the hardness variation becomes more homogeneous. This homogeneity is enhanced with the sliding distance of 10 mm in comparison with that of 5 mm. It is considered that the processing through 3 passes with 60° rotations is sufficient to develop a homogeneous microstructure.

Figure 5 shows TEM bright-field images (upper) and dark-field images (lower) with selected-area electron diffraction patterns (insets) of pure Al after HPS processing through 1, 2 and 3 passes. The dark-field images were taken with the diffracted beams indicated by arrows in the insets. Equiaxed grains with the average grain sizes of ~1 μm form after processing through 1, 2 and 3 passes but dislocations are more present in the sample after 1 pass. For the images after 2 and 3 passes, grains containing less dislocations are visible with better-defined grain boundaries. These features are consistent with hardness changes where the hardness is higher at a lower imposed strain after 1 pass but it is decreased with further straining as after 2 and 3 passes. Similar observations were also reported ealier [19—21].
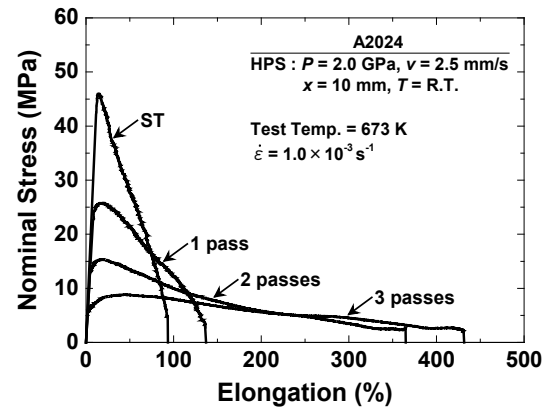
Figure 6 shows the results of tensile testing for the Al-3%Mg-0.2%Sc alloy after processing through 1, 2 and 3 passes with the sliding distance of 10 mm: (a) nominal stress-elongation curves including the one after solid solution treatment and (b) appearance after tensile deformation to failure including an undeformed specimen, for comparison. The elonagtion to failure significantly improves with the increasing numbers of passes, reaching more than 400% even after 1 pass and exceeding 1000% after 3 passes. The advent of such superplastic elongation is accompanied by the marked decrease in the maximum flow stress. It is apparent that typical superplastic flows appear with smooth and uniform
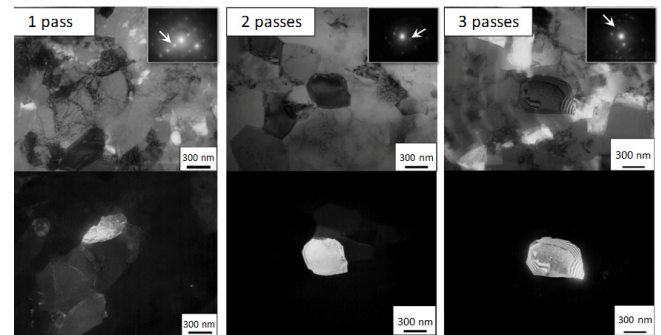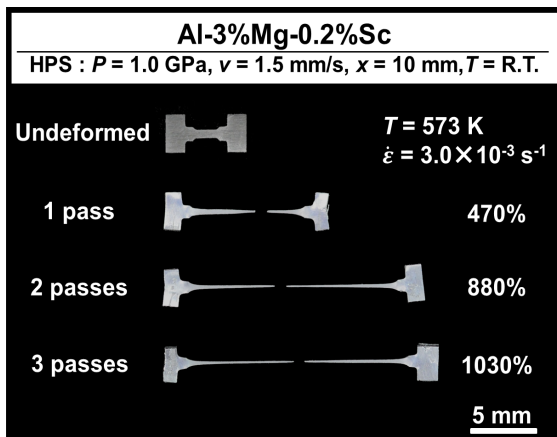

Fig. 5. TEM bright-field images (upper) and dark-field images (lower) with selected-area electron diffraction patterns (insets) of pure Al after HPS processing throgh 1 (left), 2 (middle) and 3 (right) passes. Dark-field images taken with the diffracted beams indicated by arrows in the insets. Fig. 5. TEM bright-field images (upper) and dark-field images (lower) with selected-area electron diffraction patterns (insets) of pure Al after HPS processing throgh 1 (left), 2 (middle) and 3 (right) passes. Dark-field images taken with the diffracted beams indicated by arrows in the insets.
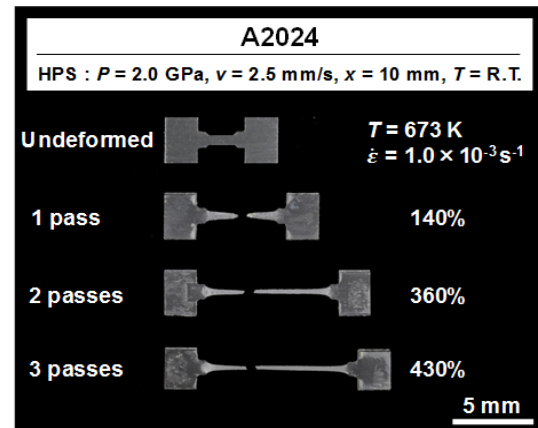

Fig. 4. OM micrographs and hardness variations throughout cross sections: (a) 2 passes with 90° rotation after sliding for 5, 10 and 15 mm and (b) 3 passes with 60° rotation after sliding for 5 and 10 mm.

a

b

Fig. 6. Results of tensile testing for Al-3%Mg-0.2%Sc alloy after processing through 1, 2 and 3 passes with sliding distance of 10 mm at room temperature: (a) nominal stress-elongation curves and (b) appearance after tensile deformation to failure.

a

b

Fig. 7. Results of tensile testing for A2024 alloy after processing through 1, 2 and 3 passes with sliding distance of 10 mm at room temperature: (a) nominal stress-elongation curves and (b) appearance after tensile deformation to failure.

elongation throughout the gauge length. This observation is well consistent with the earlier observations reported on the same alloy [22—26].

The results of tensile testing for the A2024, A7075 and AZ61 alloys are shown in Figs.7—9, respectively, where all samples were processed through 1, 2 and 3 passes with the siliding distance of 10 mm: (a) nominal stress-elongation curves and (b) appearance after tensile deformation to failure. Although the testing conditions are different, the overall trends are the same as the results of the Al-3%Mg-0.2%Sc alloy. The elongation to failure increases and the maximum flow stress decreases with the numbers of passes. It should be emphsized that the commercially available high-strength Al alloys as A2024 ans A7075 exhibit superplastic elonagtions of >400% after processing through 3 passes and and this is consistent with ealier reports [27—31]. For the AZ61 alloy, the effect of the number of HPS pass appears to be more significant than the Al alloys. The total elongation to failure is 280% after 1 pass, whereas it increases to as large as 1140% after 3 passes. There are many papers reporting superplasticity on Mg alloys using SPD processes [32—37], confirming that the HPS is an effective SPD process to produce fine-grained structures and to create superplasticity.

In order to meet the conditions for superplasticity, not only the production of small grains but also their thermal stability is important. The SPD process easily provides the former condition irrespective of the materials, particularily if the SPD process is performed under application of high pressure as HPT process. This study has demonstrated that the HPS process can also provide this ability with the sample forms of rod as well as of sheet. The Al alloys as A2024 and A7075 are higher in the strength and the Mg alloy as AZ61 is less in the ductility so that the HPS process can be pertinent to their grain refinement when the larger size of samples are required in the forms of sheet and rod. For the latter requirement concerning the thermal stablity, the Al-3%Mg-0.2%Sc alloy is the best because fine particles as Al_3Sc inhibit the grain growth as discussed earlier [22,23]. Although this study has not shown the microstructural stability with respect to temperature, some evidences are available in past publications that intermetallic particles suppress the grain growth in all of the A2024, A7075 and AZ61 alloys [27,30,37]. It is now well emphsized that the commercial high-strenth Al and Mg alloys can be promissed as potential for superplastic lightweight materials when they are processed by SPD.
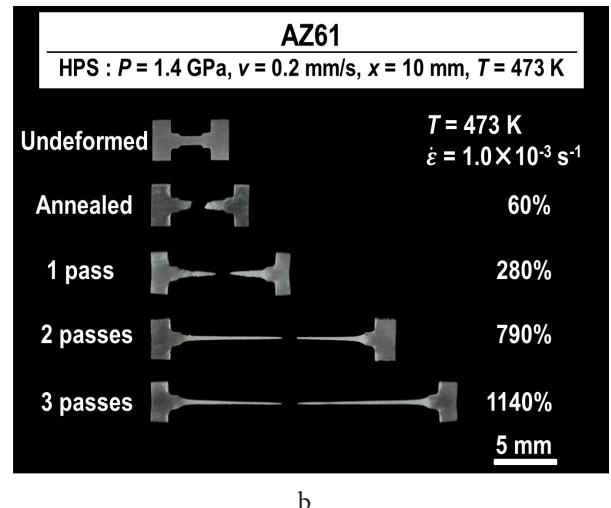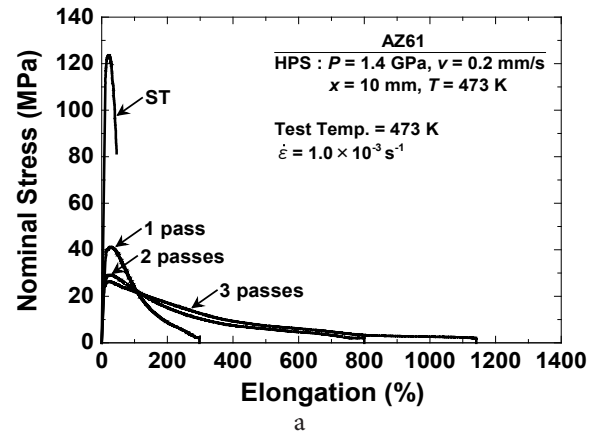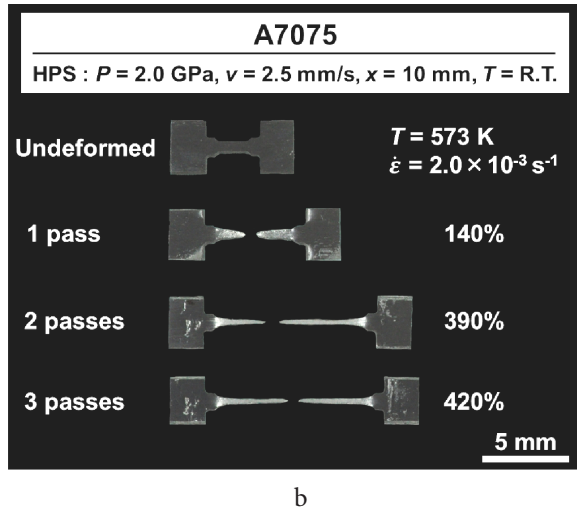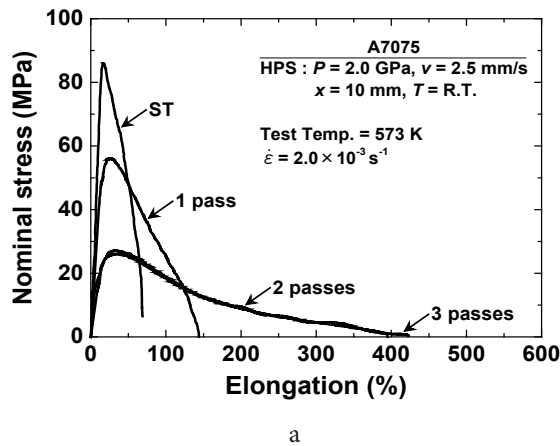
Fig. 8. Results of tensile testing for A7075 alloy after processing through 1, 2 and 3 passes with sliding distance of 10 mm at room temperature: (a) nominal stress-elongation curves and (b) appearance after tensile deformation to failure.

Fig. 9. Results of tensile testing for AZ61 alloy after processing through 1, 2 and 3 passes with sliding distance of 10 mm at 473 K: (a) nominal stress-elongation curves and (b) appearance after tensile deformation to failure.

4. Summary and conclusions

1. Grain refinement to the submicrometer range is achieved on pure Al, Al alloys (Al-3%Mg-0.2%Sc, A2024 and A7075) and a Mg alloy (AZ61) using a severe plastic deformation (SPD) process through high-pressure sliding (HPS). It is demonstrated that the HPS process originally developed for rectangular sheets is applicable to rod samples as well.

2. To obtain a homogeneous microstructure throughout the cross section of the rod, the rod sample is rotated around the longitudinal axis after each pass. Equiaxed grain structures are homogeneously developed after 3 passes with 60° rotation after each pass.

3. The Al alloys and the Mg alloy exhibit superplasticity with the total elongations of well more than 400%. In particular, the elongation to failure exceeds more than 1000% on the Al-4%Mg-0.2%Sc and AZ61 alloys.

References

1. F. A. Mohamed, T. G. Langdon, Scr. Metall. **10**, 759 (1976).
2. R. Z. Valiev, R. K. Islamgaliev, I. V. Alexandrov, Prog. Mater. Sci. **45**, 103 (2000).
3. R. Z. Valiev, Y. Estrin, Z. Horita, T. G. Langdon, M. J. Zehetbauer, Y. T. Zhu, JOM **58** (4), 33 (2006).
4. R V. M. Segal, V. I. Reznikov, A. E. Drobyshevskiy, V. I. Kopylov, Russian Metall. **1**, 99 (1981).
5. Y. Saito, H. Utsunomiya, N. Tsuji and T. Sakai, Acta Mater. **47**, 579, (1999).
6. P. W. Bridgman, Phys. Rev. **48**, 825 (1935).
7. T. Waitz, V. Kazykhanov and H. P. Karnthaler, Acta Mater. **52**, 137 (2004).

8. Y. Ikoma, K. Hayano, K. Edalati, K. Saito, Q. Guo and Z. Horita, Appl. Phys. Lett. **101**, 121908 (2012).

9. K. Edalati, J. Matsuda, H. Iwaoka, S. Toh, E. Akiba and Z. Horita, Int. J. Hydrogen Energy **38**, 4622 (2013).

10. K. Edalati and Z. Horita, J. Mater. Sci. **45**, 4578 (2010).

11. K. Edalati and Z. Horita, J. Mater. Sci. **47**, 473 (2012).

12. G. Sakai, K. Nakamura, Z. Horita, T. G. Langdon, Mater. Sci. Eng. **A406**, 268 (2005).

13. L. S. Toth, M. Arzaghi, J. J. Fundenberger, B. Beausir, O. Bouaziz, R. Arruffat-Massion, Scr. Mater. **60**, 175 (2009).

14. J. T. Wang, Z. Li, J. Wang, T. G. Langdon, Scr. Mater. **67**, 810 (2012).

15. A. Hohenwarter, Mater. Sci. Eng. **A626**, 80 (2015).

16. T. Fujioka, Z. Horita, Mater. Trans. **50**, 930 (2009).

17. K. Tazoe, S. Honda and Z. Horita, Mater. Sci. Forum **667—669**, 91 (2011).

18. S. Lee, K. Tazoe, I. F. Mohamed and Z. Horita, Mater. Sci. Eng. **A628**, 56 (2015).

19. C. Xu, Z. Horita and T. G. Langdon, Acta Mater. **55**, 203 (2007).

20. Y. Harai, Y. Ito and Z. Horita, Scr. Mater. **58**, 469 (2008).

21. Y. Ito and Z. Horita, Mater. Sci. Eng. **A503**, 32 (2009).

22. S. Komura, M. Furukawa, Z. Horita, M. Nemoto, T. G. Langdon, Mater. Sci. Eng. **A297**, 111 (2001).

23. S. Komura, Z. Horita, M. Furukawa, M. Nemoto, T. G. Langdon, Metall. Mater. Trans. A **32A**, 707 (2001).

24. G. Sakai, Z. Horita, T. G. Langdon, Mater. Sci. Eng. **A393**, 344 (2005).

25. Z. Horita and T. G. Langdon, Scr. Mater. **58**, 1029 (2008).

26. Y. Harai, K. Edalati, Z. Horita, T. G. Langdon, Acta Mater. **57**, 1147 (2009).

27. S. Lee, M. Furukawa, Z. Horita, T. G. Langdon, Mater. Sci. Eng. **A342**, 294 (2003).

28. I. Charit, R. S. Mishra, Mater. Sci. Eng. **A359**, 290 (2003).

29. S. V. Dobatkin, E. N. Bastarache, G. Sakai, T. Fujita, Z. Horita, T. G. Langdon, Mater. Sci. Eng. **A408**, 141 (2005).

30. A. Alhamidi, Z. Horita, Mater. Sci. Eng. **A622**, 139 (2015).

31. S. Lee, Z. Horita, Mater. Sci. Forum **794—796**, 807 (2014).

32. Z. Horita, K. Matsubara, K. Makii, T. G. Langdon, Scr. Mater. **47**, 255 (2002).

33. H. Somekawa, H. Hosokawa, H. Watanabe, K. Higashi, Mater. Sci. Eng. **A339**, 328 (2003).

34. Y. Miyahara, Z. Horita, T. G. Langdon, Mater. Sci. Eng. **A420**, 240 (2003).

35. J. A. del Valle, F. Carreño, O. A. Ruano, Scr. Mater. **57**, 829 (2007).

36. R. B. Figueiredo, T. G. Langdon, J. Mater. Sci. **43**, 7366 (2008).

37. Y. Harai, M. Kai, K. Kaneko, Z. Horita, T.G. Langdon, Mater. Trans. **49**, 76 (2008).